Ferroelectric PZT RF MEMS Resonators

Jeffrey S. Pulskamp, Sarah S. Bedair, Ronald G. Polcawich, Daniel Judy
US Army Research Laboratory
Adelphi, MD, USA

Sunil A. Bhave
School of Electrical and Computer Engineering
Cornell University
Ithaca, NY, USA

***Abstract*—This paper presents recent work on ferroelectric-piezoelectric lead zirconate titanate (PZT) RF MEMS resonators. Several research topics are introduced including design modifications that improve out-of-band rejection by 35dB, a demonstration of a high rejection (~117dB) parallel resonant mode with DC bias tunable rejection, a MEMS support design for the mitigation of anchor loss, and a numerical electrode shaping design technique that permits the excitation of arbitrary modes in arbitrary geometries.**

I. Introduction

Piezoelectric transduction via PZT offers a number of unique advantages for RF MEMS applications. It offers extremely low power consumption and low voltage device operation [1]. CMOS compatible voltages in RF MEMS switches have been previously demonstrated [2]. Due to the strong piezoelectric effect in PZT, actuators are capable of very large force generation and or large displacements. This provides advantages in devices like RF MEMS switches where large forces lead to low contact resistance/insertion loss and improved lifetime and large displacements lead to improved high frequency isolation. These actuation capabilities are a consequence of the large electromechanical coupling factors and piezoelectric coefficients of the material. PZT has coefficients that are generally an order of magnitude larger than those of AlN or ZnO [3]. PZT is not only a piezoelectric material but also possesses ferroelectric properties. The high electric field response in ferroelectrics permits the tuning of the dielectric, elastic, piezoelectric, and coupling factors of PZT [4]. This permits the advantageous DC-bias tuning of frequency and motional impedance in RF MEMS resonators based on ferroelectrics like PZT [5].

Thin film piezoelectrics tend to have much higher breakdown strengths than their bulk counterparts. This permits the safe application of actuation or bias fields that are well in excess of the coercive field of the PZT. Consequently, significant high electric field nonlinearity and hysteresis are observed in thin films that are rarely encountered in bulk PZT actuator applications. At these high electric fields, PZT exhibits the traditional ferroelectric hysteresis loop relating electric polarization and field. The dielectric and piezoelectric coefficients display a similar nonlinear response [6]. The combination of the piezoelectric and dielectric nonlinearity leads to tuning of the various quasi-static electromechanical coupling factors; such that high DC biasing provides significant improvements in electromechanical coupling.

Despite the long and successful history of bulk PZT resonators [7]; drawbacks to PZT, particularly at higher frequency operation, have discouraged the exploitation of this strong piezoelectric in thin films and MEMS. PZT does have high mechanical and dielectric loss and the temperature stability of the dielectric, ferroelectric, and piezoelectric properties can pose challenges. Despite these challenges, there exist several key and unique advantages for utilizing PZT in RF MEMS resonator applications. The strong piezoelectric coefficients and material coupling factors permit wide-bandwidth and low motional resistances in filters and high efficiency and voltage gain in electromechanical MEMS power transformers [8]. The high field ferroelectric response permits interesting opportunities to tune and/or trim resonators with DC bias. High levels of device integration have also been demonstrated in PZT RF MEMS, including one of the first demonstrations of monolithically integrated switches and filters [9]. Previous work demonstrated the advantages of integrating thin film PZT with high mechanical quality factor single crystal silicon, or PZT-on-Si resonator technology, to create an effective thin film composite piezoelectric material [5]. By utilizing the PZT as the transducer and the silicon as the primary resonator structure, favorable tradeoffs exist between the mechanical quality factor of the silicon and the effective coupling factor of the resonators. Despite the reduced effective coupling, the improvements in quality factor generally lead to not only higher Q but also to reduced motional resistance.

The remainder of the paper introduces some recent research in PZT-based RF MEMS resonators. Section II addresses the improvement of out-of-band rejection in two-port PZT resonators. Section III presents the demonstration of a high rejection (~117dB) and tunable parallel resonant mode. Section VI introduces a novel MEMS support design technique for the mitigation of anchor loss. Section V introduces a numerical electrode shaping design technique that permits the excitation of arbitrary modes in arbitrary geometries and Section VI concludes the paper.

II. Improving Out-of-Band Rejection

Improving out-of-band rejection in resonant filters is necessary for reducing the interference from unwanted signals. An illustration of a previously designed length extensional mode, PZT-on-silicon resonator design is shown in Fig. 1(a). A high isolation device type is also illustrated where the drive

and sense common bottom electrode is etched with the fabrication process previously developed [10]. This PZT/Pt etch feature is illustrated in Fig. 1(b). Equivalent circuit models, including the device parasitics, are shown in Fig. 2(a-b). These correspond to the illustrations in Fig. 1(a-b), respectively. The resistance, R_g, arising from the routing of the bottom platinum in the tethers to the ground plane is proportional to the tether length/width. It is important to note that this resistance has a significant effect on the stop-band performance of the resonant device. This R_g value is particularly important to consider with the high dielectric constant of PZT. At high frequencies, current can flow out of node A through the sense capacitance, due to the low impedance of C_{sense}, manifesting itself as "feed-through" current in the frequency response.

Three fabricated device types are under consideration. The first (type-I) is a high feed-through device with R_g = 1.7 Ω, the second (type-II) is a high feed-through device with R_g = 15 Ω, and the third (type-III) is a low feed-through, high isolation device with R_g = 1.7Ω. The length, L_{elec}, width, w_{elec}, of both devices' top electrodes (Fig. 1(b)), and gap in the PZT and platinum, w_{gap}, are 196 µm, 14 µm, and 4 µm, respectively. The device length, L_{tot}, and width, w_{tot}, are 200 µm and 40 µm, respectively. The platinum thickness is 100 nm, the device silicon is 10 µm, and the PZT is 0.5 µm. The measured S-parameter (S_{21}) frequency responses for the device types in the 1-200MHz range are shown in Fig. 3. The devices have been de-poled to illustrate the purely electrical feed-through. An improvement of 35dB (type-I versus type-III) in the stop-band is measured at 200MHz. A 16 dB degradation in the stop-band rejection, consistent with theory, results for the device with larger R_g (15 Ω versus 1.7 Ω). This confirms the importance of this parasitic as a relevant device parameter. Further minimizing this parasitic may be achieved through modified tether design (Section IV) and fabrication steps to improve both resonator insertion loss as well as high frequency stop-band rejection.

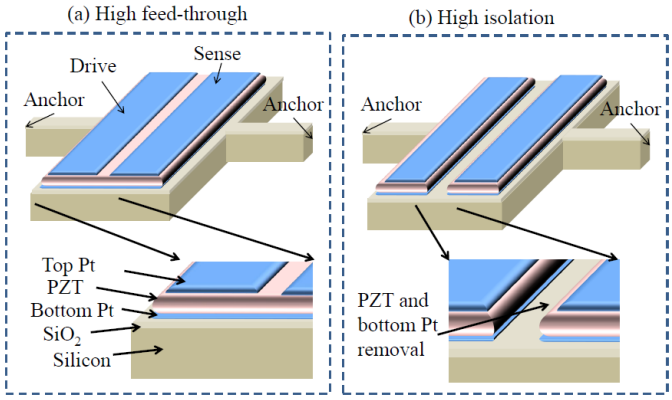

Figure 1: (a) 3D illustration of high feed-through, low isolation resonator device fabricated through a PZT-on-silicon process [10]. (b) Illustration of the high isolation device where PZT and the bottom platinum are etched in the region between the drive and sense electrode.

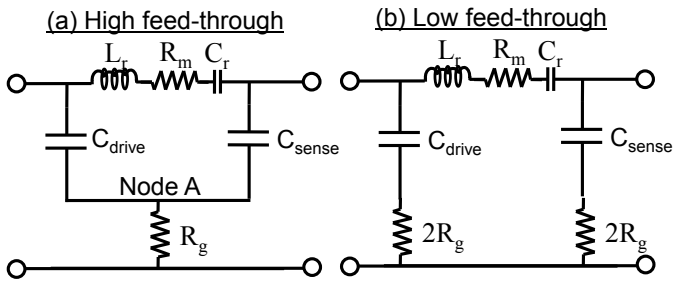

Figure 2: (a) Equivalent circuit of the two port resonant device of Fig.1(a) including the routing parasitics and electrically equivalent representation of R_m, C_r and L_r of the mechanical response (b) equivalent circuit of device with etch feature as illustrated in Fig. 1(b).

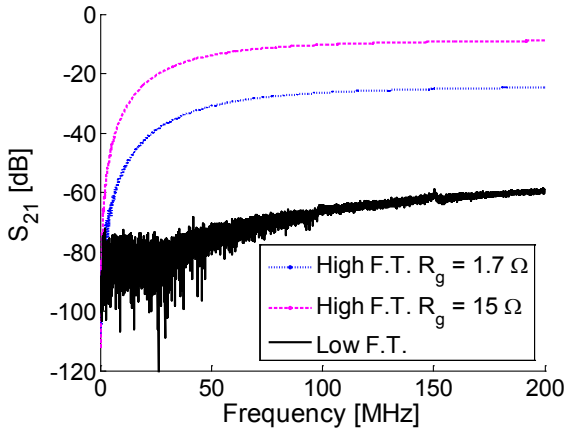

Figure 3: Frequency response of device with (low F.T.) and without (high F.T.) the PZT/Pt cut on the resonator.

III. High Q Parallel Resonances

In addition to the utility of RF MEMS resonators for band-pass filter applications; they may also be used as high rejection, parallel resonators, in band-stop or notch filter applications. The following illustrates that the existence of high rejection, parallel resonances are a consequence of the cancellation of motional and feed-through currents. For the current analysis, the following frequency dependent impedances will be used: $Z_r(s)$, the motional impedance of the resonator, $Z_d(s)$, the impedance of the drive capacitance, $Z_s(s)$, the impedance of the sense capacitance, and $Z_L(s)$ the load impedance of the measurement instrument (50 Ω). The drive and sense capacitances are illustrated in Fig. 1(a). The complex variable, s, is represented by $j\omega$, where ω is the frequency in [rad / sec]. Assuming $Z_r(s) >> Z_L(s)$, the ratio of the motional current, $i_r(s)$, to feed-through current, $i_f(s)$, current is

$$\frac{i_r(s)}{i_f(s)} \approx \frac{1}{Z_r(s)}\left(Z_d(s)\left(1+\frac{Z_s(s)+Z_L(s)}{R_g}\right)+1\right) \quad (1)$$

The conditions for parallel resonance are achieved with +/- 180° phase and unity magnitude for the above expression which leads to current cancellation of the motional with the feed-through current.

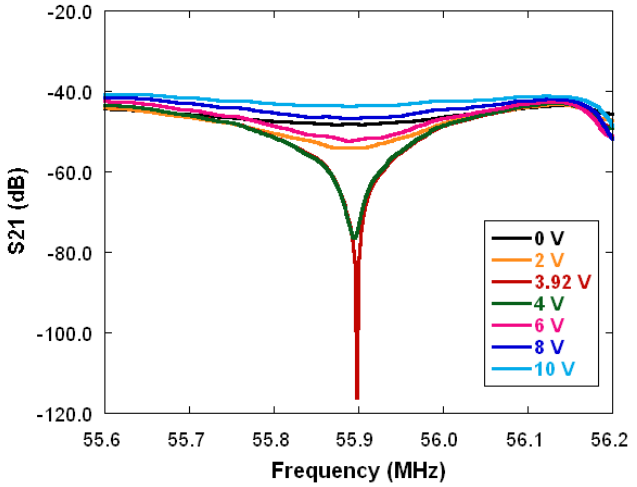

Figure 4: Frequency response of device with a high feed-through design under various DC bias conditions. High rejection parallel resonance is observed when the resonator motional exactly cancels the feed-through current.

For a device similar to that described above in Fig. 1(a), a high rejection parallel resonance mode was identified. The measured frequency response is shown in Fig. 4. A DC bias is superimposed on the AC signal at both the input and output ports using bias-tees. A high isolation of 117 dB is measured with a 3.92V DC bias at 55.9 MHz. The pass-band insertion loss is measured as 45dB at 55.6 MHz. Through DC bias tuning of the ferroelectric PZT properties, a quasi-infinite isolation can be achieved through proper design of the resonator motional impedance and the finite resistance to ground, R_g, which was introduced in Section II.

IV. Anchor Loss Reduction

Anchor loss has long been known to be a potential limiting mechanical loss mechanism. Integration of PZT with single crystal silicon enables dramatically higher quality factors than are achievable with PZT alone and anchor loss may eventually limit resonator quality factors. The common solution in MEMS resonators and older wire supported quartz and ceramic resonators is quarter-wave acoustic matched support design [11]. Quarter-wave support design views the support structure as a mechanical impedance transformer [12]. The support should accommodate some velocity at the attachment location between the tether and the resonator (drive point) and provide a large mechanical impedance at the attachment location with the substrate (anchor point). However, in an actual continuous elastic structure, there is always the potential for stress concentration at the anchor point. Therefore anchor loss can be further reduced by minimizing the amount of strain energy present near the anchor point that could potentially radiate into the substrate.

A conservative estimate of the anchor loss quality factor (anchor Q) may be obtained by assuming all of the strain energy present at the anchor point will be completely radiated during a given vibration cycle. This implies that no acoustic energy is reflected back into the resonator due to scattering of

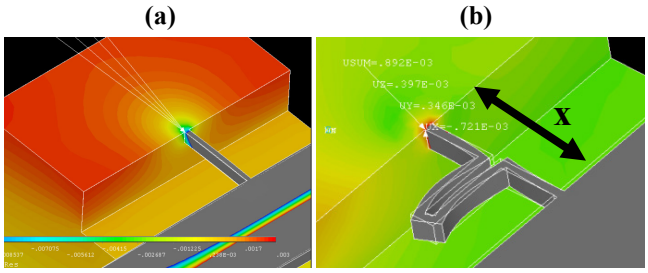

Figure 5: (a) Displacement modal analysis of a 200μm x 40μm free-free beam resonator operating at the fundamental length extensional mode (23.1 MHz). The resonator is supported by a straight 20μm long x 2μm wide tether. (b) Modal analysis of the same resonator as in (a) but with an alternative tether design. The beam resonator is visible in the lower right of both figures. The plotting contours highlight the response in the substrate.

acoustic waves radiated during prior vibration cycles. This assumption will result in predicting a lower bound to the quality factor. The anchor Q is merely the ratio of 2π times the stored mechanical energy in the resonator to the acoustic energy radiated into the substrate per period. As strain energy is proportional to the square of the strain, the conservative estimate for the anchor Q is proportional to the inverse of the square of the strain at the anchor point.

In contrast to modeling anchor loss via harmonic analysis [13], modal analysis is far less computationally demanding for the same physical model but only provides relative kinematic and dynamic data. However dissimilar support designs can be compared if the modal data of the two designs are scaled with a consistent normalization scheme; for example by normalizing both modeshapes to unity. The ratio of the squares of the modal strains of the two designs will be equal to the ratio of their anchor Qs (lower bound).

Fig. 5(a) illustrates a typical MEMS straight tether support, and Fig. 5(b) illustrates a potentially more compliant support. The results are from an ANSYS 12.0 FEA modal analysis of the same resonator at its fundamental length extensional mode of 23.1 MHz. As can be seen in Fig.s 5(a-b), the different tethers are experiencing different "local" vibrations, at the identical resonator mode, which provide different anchor loss conditions. The tether in Fig. 5(b) actually has an average absolute value of the relative Von Mises stress at the surface between the tether and the substrate that is 89% lower than that of the straight tether design in Fig. 5(a).

This difference in these tether responses can be understood by considering the frequency response and modal data of the isolated tether. The tether structure behaves essentially as its own resonator with dynamics, partly determined by the boundary conditions imposed by the substrate and resonator, and excitation imposed by the motion of the resonator at the drive point. At a given frequency, the motion of the tether will be some linear combination of the "local" tether modes of vibration. Tether modes with low mechanical impedances at the drive point, subjected to large relevant forces by the motion of the resonator, will be the dominant tether modes governing the dynamics of the tethers, at any given frequency. The goal of any design approach is to determine

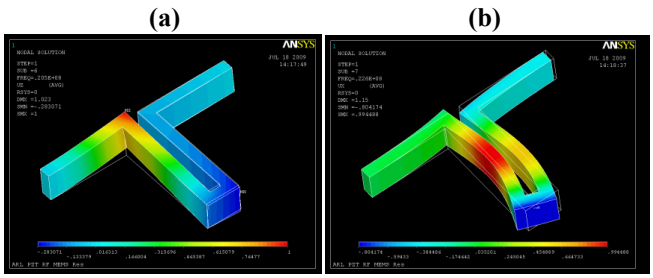

Figure 6: Modal analysis of isolated tether under boundary conditions consistent with substrate and resonator attachments impedances. The plotted response is the vector-sum of displacements (unity normalized).(a) 21.2 MHz tether mode (b) 22.6 MHz tether mode.

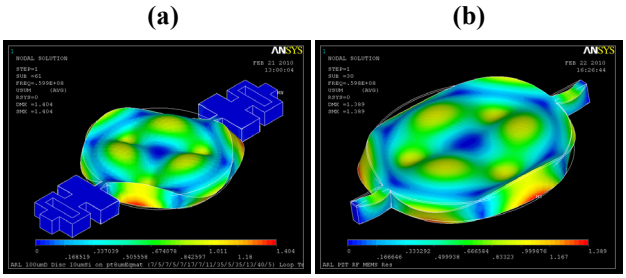

Figure 7: Modal analysis of 100µm diameter PZT-on-Si disc resonator operating at 60 MHz high order disc flexure mode. The plotted response is the vector-sum of unity normalized displacements (blue identifies near zero relative displacements). (a) New transformer design (b) 20µm long x 5µm wide straight tether design.

what tether modes will dominant the dynamics of the tethers at the desired resonator operating frequency. Generally, the supports can be designed by considering the isolated tether clamped at the anchor point and then by defining mechanical boundary conditions at the drive point that are compatible with the relevant mechanical impedances presented by the resonator.

For example, the drive point of the length extensional mode free-free beam resonator of Fig.s 5(a-b), present x-direction finite displacements to the tethers. Consequently, the relevant mechanical impedance is that of the ratio of the x-direction translational velocity to axial forces in the same direction. The isolated tether was simulated with a clamped boundary condition at the anchor point and the drive point was constrained to only permit x-direction displacements.

Fig. 6(a) and Fig. 6(b) illustrate two modeshapes of the tether from Fig. 5(b) that have resonant frequencies within a few MHz of the main free-free resonator frequency (23.1 MHz). The mode in Fig. 6(a) displays a much higher mechanical impedance (less motion at the drive point – right side of tethers in Fig. 6) than the mode in Fig. 6(b). Comparison of Fig. 6(b) with Fig. 5(b) reveals that the 22.6 MHz isolated tether mode is the dominant "local" tether mode present in the tether at the resonators resonant length extensional mode of 23.1 MHz.

Utilizing this approach for design involves determining a desired resonator geometry and mode, determining the relevant mechanical impedances of the tether attachment locations, and simulating a given tether design with the appropriate boundary conditions. The average values of the stresses on the surface between the substrate and the tether (anchor surface) are calculated and compared for the various tether modes. Once a low average stress mode is selected, the tether dimensions are resized so that it is the dominant local tether mode at the desired resonator frequency.

This technique was used to design the resonator support seen in Fig. 7(a). To compare this design with a typical MEMS straight tether design, a 20µm x 5µm straight tether (Fig. 7(b)) was simulated with a 100µm diameter silicon disc resonator with a similarly sized new mechanical impedance transformer design. The tether dimensions were fixed without constantly matching for each resonator mode to assess the bandwidth sensitivity of the designs. The average

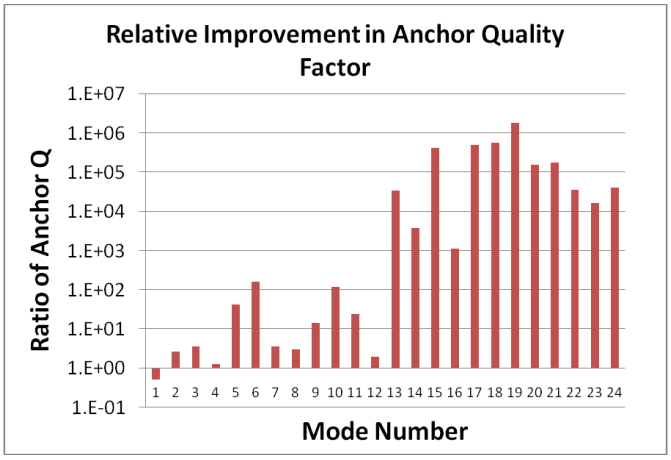

Figure 8: Plot of anchor Q ratio (mechanical transformer design Q / straight tether design Q) for the first 24 disc modes. The anchor Q ratio is the ratio of the squares of the average anchor surface stresses.

of the absolute value of the Von Mises stress on the anchor surface was calculated for each mode in each case. Fig. 8 plots the ratio of the anchor Q (lower bound) for the straight and transformer tether designs for the first 24 disc modes. In all but the first case, there are multiple order of magnitude improvements in the anchor Qs between the two designs, particularly for higher frequency modes. Fig. 7(a-b) plots the modal displacements for an example 60 MHz disc mode. The improved theoretical performance of the transformer tether design is apparent between Fig. 7(a) and 7(b) where the transformer tether exhibits virtually no displacements. Nearly all of the disc modes from about 15 MHz through ~200 MHz (upper frequency limit of simulation) display similar anchor performance as Fig. 7(a). The predicted performance difference suggests that the transformer based design dramatically reduces the anchor loss, is less sensitive to the matching requirements of quarter-wave designs (superior performance over a wide range of frequencies without resizing), and permits larger geometries that can reduce the tether parasitics described in Section II.

V. ELECTRODE SHAPING

The drive to achieve insertion losses and quality factors consistent with commercializing MEMS resonator technologies have led to a research focus on minimizing motional resistances and maximizing quality factors. In addition to achieving further improvements in these metrics, there remains a need to improve the suppression of spurious vibrational modes, increase resonant frequencies, improve power handling and linearity, and achieve wider bandwidth resonators for band select filter applications. The proper design of the resonator electrodes to selectively excite and detect desired modes, or "electrode-shaping", can provide improvements in these performance metrics. There has been an extensive body of research in electrode-shaped transducers, particularly for applications in active vibration control of structures [14].

Optimal excitation and detection electrodes may be analytically derived for simple one-dimensional modes by utilizing the orthogonality property of the vibrational modeshapes [15]. However, extending this technique to more complicated modes is difficult but extending the theory to higher dimensional modes, such as those existing in discs, poses considerable complications. In addition, to determine electrode-shapes in arbitrary cases, numerical techniques are required to treat issues such as nontrivial geometries, modes not conveniently described by analytical models, deformation coupling effects in asymmetric composites, anisotropic material properties, and the influence of non-optimal tether conditions on the modeshapes.

An alternative to the traditional approach is to determine the local suitability of placing an electrode on the resonator. The electrode shapes are then ascertained from maps of this local determination of electrode placement. For excitation, maximizing the local strain leads to maximizing the local contribution to the lumped equivalent excitation force, or modal force. Therefore, we may determine the local suitability of electrode placement by considering strain compatibility between the excited piezoelectric and the desired mode at each location on the resonator. The mode is excited locally when the piezoelectrically induced stresses are consistent with the modal stresses; for example when the piezoelectric material is assumed to be in compression, it will excite regions of the resonator for modes where that location is also simultaneously in a state of compression.

This technique does not necessarily maximally excite the desired mode or maximally suppress unwanted modes, but rather determines electrode shapes that ensure the desired mode is excited and detected. For this scenario, the excitation electrode shape for a particular mode may be determined by finding those locations where the e_{31} and e_{32} piezoelectric stress constants both excite or inhibit the mode. For PZT, these are the locations where the two modal principle stress components have the same sign. For locations where the two modal principle stress components have dissimilar signs, some degree of force cancellation occurs and these locations are neglected. The determination of the detection electrode shape consists of solving the constitutive equation for the direct piezoelectric effect locally for the differential of the induced charge.

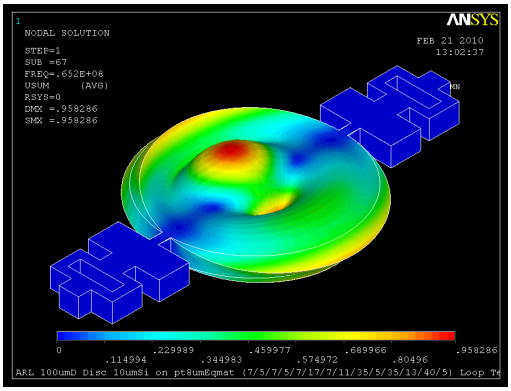

Figure 9: FEA modal analysis of an example electrode-shaped device, a high order flexure disc mode (100μm diameter). The plotted response is the vector-sum of displacements (unity normalized).

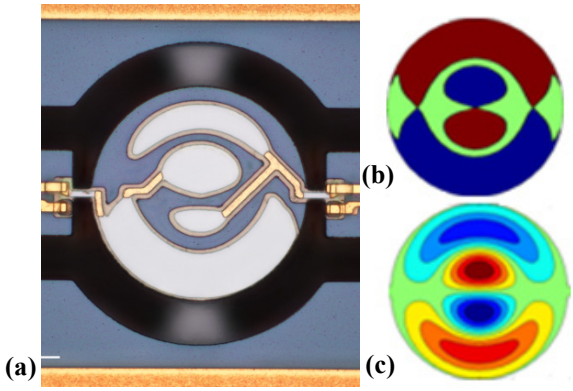

Figure 10: (a) Micrograph of the fabricated two-port PZT-on-Si disc resonator electrode-shaped for the mode illustrated in Fig. 9. The intended excitation port is on the left side of the image (b) Model result for excitation electrode shape. (c) Model result for detection electrode shape.

This technique was implemented with numerical modal analysis in ANSYS 12.0, MATLAB data processing and scripted automatic CAD generation. To validate the technique, sixteen different disc modes were designed as two-port devices and characterized. The device fabrication and layer thicknesses were previously described in Section II. The fabricated resonators were tested in an RF probe station at atmospheric pressure. Full S-parameter matrices were extracted for each resonator using a Rohde & Schwarz ZVB vector network analyzer.

Fig. 9 illustrates the modeshape of an example device, a high order flexure mode. Fig. 10(a) is a micrograph of the fabricated device; Fig. 10(b) displays the results of the electrode-shaping technique for the excitation electrode; and Fig. 10(c) displays the results of the technique for the detection electrode for the two-port devices. The red and blue regions of Fig. 10(b) correspond to the two possible excitation electrode locations. These locations correspond to either tensile or compression regions of the modal analysis simulation and either location may be chosen. The red and blue graded regions visible in Fig. 10(c) display the locations for the detection electrode. These locations correspond to either positive or negative charge regions of the modal analysis simulation and again, either may be chosen. However, in both the excitation and detection cases, electrodes

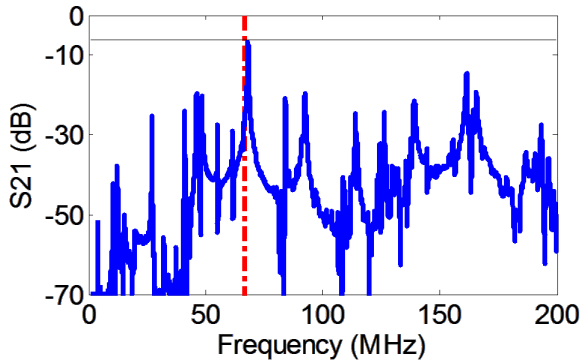

Figure 11: Experimental results for the transmission frequency response of the device shown in Fig. 10(a). The dashed red line identifies the design frequency.

that overlap the two different regions will experience some degree of force or charge cancellation, respectively. Fig. 11 displays the frequency response of the measured forward transmission coefficient S_{21} for the device shown in Fig. 10(a), displaying an unmatched (50Ω terminated) insertion loss of 6.6 dB. The dashed red line indicates the design resonant frequency for the intended mode at 68 MHz. The proximity of the lowest loss mode to the design frequency suggests the electrode shape is successfully exciting the desired mode.

To more fully characterize the electrode-shaped resonators, the measured S_{21} peak values within ±4% of *each* design frequency were determined for *each* resonator. The difference between the peak S_{21} of a given design and the average of all of the other resonators, within the same ±4% search window, provides a measure of the how well a particular electrode-shape is performing. Fig. 12 is a stem plot of this difference for each of the 16 different electrode designs for the disc resonators. The average across the different disc designs yields an average improvement in S_{21} for the shaped designs of 18.1 dB and a maximum improvement of 44.3 dB.

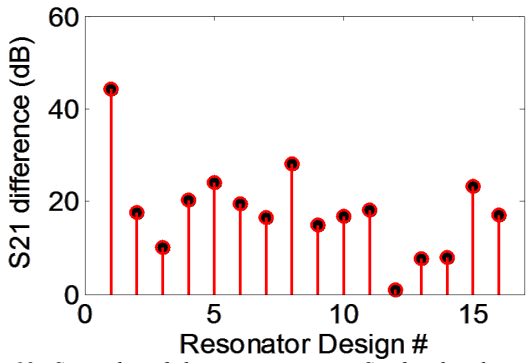

Figure 12: Stem plot of the improvement in S_{21} for the electrode-shaped designs, relative to all other electrode designs (same resonator geometry). Each value represents the improvement in insertion loss of that mode relative to the average of the other designs within ±4% of the design frequency.

VI. Conclusions

In summary, this paper introduced several research topics related to piezoelectric-ferroelectric PZT RF MEMS resonators. Significant improvements in out-of-band rejection (>35 dB), consistent with theory, were demonstrated by isolating the bottom electrodes of the excitation and detection transducers of two-port piezoelectric resonators. A high rejection (~117dB) parallel resonant mode was demonstrated with the benefit of the tunable ferroelectric properties of PZT-on-silicon resonators via high field DC bias. A MEMS support design technique, utilizing modal analysis, for the mitigation of anchor loss was presented. A theoretical comparison illustrated mechanical transformer-based tether designs derived from this technique, can provide orders of magnitude lower anchor loss than a more traditional MEMS straight support design. A numerical electrode shaping design technique was demonstrated to permit the excitation of arbitrary modes in disc geometries. The average improvement in S_{21} for the electrode-shaped designs was 18.1 dB relative to all other electrode designs for the same resonator geometry and a maximum improvement of 44.3 dB were demonstrated.

Acknowledgment

The authors wish to thank Brian Power and Joel Martin (Army Research Lab) for the fabrication.

References

[1] S. Trolier-McKinstry and P. Muralt, "Thin Film Piezoelectrics for MEMS," J. Electroceramics, vol. 12, pp. 7 – 17, 2004.

[2] R. G. Polcawich, J. S. Pulskamp, D. Judy, P. Ranade, S. Trolier-McKinstry, and M. Dubey, "Surface micromachined microelectromechanical ohmic series switch using thin-film piezoelectric actuators," IEEE Transactions Microwave Theory and Techniques, vol. 55, no. 12, pp. 2642 – 2654, 2007.

[3] R. Ghodssi, Reza and P. Lin, *MEMS Materials and Processes Handbook.* New York: Springer, 2011.

[4] A. Tagantsev, V. Sherman, K. Astafiev, J. Venkatesh, and N. Setter, "Ferroelectric Materials for Microwave Tunable Applications," J. of Electroceramics, vol. 11, pp. 5–66, 2003.

[5] H. Chandrahalim, S. A. Bhave, R. Polcawich, J. Pulskamp, D. Judy, R. Kaul, and M. Dubey, "Performance comparison of $Pb(Zr0.52Ti0.48)O3$-only and $Pb(Zr0.52Ti0.48)O3$ -on-silicon resonators," Applied Physics Letters 93(23), p. 233504, 2008.

[6] A. Kholkin, E. Akdogan, A. Safari, P.Chauvy and N. Setter, "Characterization of the effective electrostriction coefficients in ferroelectric thin films," J. Appl. Phys. vol. 89, no. 12, pp. 8066-8073, 2001.

[7] S. Fujishima, "The History of Ceramic Filters", IEEE Trans. UFFC, vol. 47, no. 1, pp. 1-7, January 2000.

[8] S. Bedair, J. Pulskamp, B. Morgan, and R. Polcawich, "Performance model of electrode tailored thin film piezoelectric transformers for high frequency switched mode power supplies," Power MEMS 2009, Silver Spring, Maryland, pp. 435-438, Dec. 1 - 4, 2009.

[9] J. Pulskamp et al., "Monolithically integrated piezoMEMS SP2T switch and contour-mode filters," MEMS 2009, pp. 900-903.

[10] H. Chandrahalim, et. al., "Influence of silicon on quality factor, motional impedance, and tuning range of PZT-transduced resonators," *2008 Solid State Sensor, Actuator and Microsystems Workshop*, Hilton Head Island, SC, pp. 360-363, 2008.

[11] R. A. Johnson, *Mechanical Filters in Electronics*. New York: Wiley, 1983.

[12] K. Wang, Y. Yu, A. Wong and C. Nguyen, "VHF free–free beam high-Q micromechanical resonators," IEEE/ASME J. Microelectromech. Syst., vol. 9, no. 3, pp. 347–360, Sep. 2000.

[13] M. Pandey, R. Reichenbach, A. Zehnder, A. Lal and H. Craighead, "Reducing anchor loss in MEMS resonators using mesa isolation," JMEMS, vol. 18, no. 4, pp. 836-844, August 2009.

[14] M. Frecker, "Recent advances in optimization of smart structures and actuators," J. Intell.Mater. Syst. Struct. 14 207–16, 2003.

[15] A. Prak, M. Elwenspoek, and J. Fluitman, "Selective mode excitation and detection of micromachined resonators," J. Microelectromech. Syst., vol. 1, no. 4, pp. 179–186, Dec. 1992.